Contents lists available at ScienceDirect

Journal of Saudi Chemical Society

journal homepage: www.ksu.edu.sa

Tuning the photovoltaic potential of thiazole based materials via incorporation of selenophene and electron acceptors rings at peripheral positions: A DFT approach

Muhammad Khalid [a,b,*], Sadia Jamal [a,b], Ataualpa Albert Carmo Braga [c], Muhammad Haroon [d], Rajeh Alotaibi [e], Ke Chen [f,**]

[a] Institute of Chemistry, Khwaja Fareed University of Engineering & Information Technology, Rahim Yar Khan 64200, Pakistan
[b] Centre for Theoretical and Computational Research, Khwaja Fareed University of Engineering & Information Technology, Rahim Yar Khan 64200, Pakistan
[c] Departamento de Química Fundamental, Instituto de Química, Universidade de São Paulo, Av. Prof. Lineu Prestes, 748, São Paulo 05508-000, Brazil
[d] Department of Chemistry and Biochemistry, Miami University, Oxford, OH, USA
[e] Department of Chemistry, College of Science, King Saud University, Riyadh 11451, Saudi Arabia
[f] Department of Infectious Diseases, The Affiliated Hospital of Southwest Medical University, Luzhou 646000, China

ARTICLE INFO

Keywords:
Chlorothiazole
Selenophene
DFT
Frontier molecular orbitals
Open circuit voltage

ABSTRACT

The non-fullerene acceptor (NFA) chromophores have sparked scientific and economic interest, due to their rapid advancements in power conversion efficiencies. Therefore, a series of new chlorothiazole based compounds **(STM1-STM6)** with A1–π–A2–π–A1 configuration was designed using reference chromophore **(STMR)**. Structural modifications were made *via* incorporating selenophene and extended acceptor units, to enhance photovoltaic response in the designed materials. Density functional theory/time dependent-density functional theory (DFT/TD-DFT) calculations were executed at M06/6-311G (d,p) level to investigate key electronic and photovoltaic properties of **STM1-STM6**. So, various analyses such as UV–Visible, frontier molecular orbitals (FMOs), transition density matrix (TDM), density of states (DOS), open circuit voltage (V_{oc}) and binding energy (E_b) were conducted to comprehend the photovoltaic properties. The designing in structural aspects with terminal acceptors and π-linker induced a reduction in energy gaps (ΔE = 2.078–2.237 *eV*) with an enhancement in the bathochromic shift (λ_{max} = 744.650–798.250 *nm* in chloroform) than reference compound. A higher exciton dissociation rate was observed in all the compounds due to lower binding energy values (E_b = 0.525–0.572 *eV*). Additionally, TDM and DOS findings further endorsed the effective charge delocalization from HOMO to LUMO. Among all the examined compounds, **STM3** exhibited the smallest band gap (2.078 *eV*), highest absorption maxima (798.250 *nm*), and the lowest exciton binding energy (0.525 *eV*), indicating significant electronic properties. Moreover, V_{oc} analysis was conducted with respect to $HOMO_{PBDBT}$-$LUMO_{acceptor}$ for all the designed chromophores; consequently, **STM2** demonstrated a substantial V_{oc} value of 1.647 *V*. Similarly, electron hole analysis was also conducted and significant electron and hole density was observed in all the investigated compounds, especially in **STM2**. The entitled compounds with photovoltaic potential would be considered as promising materials for the development of solar energy devices.

1. Introduction

Currently, one of the major global concerns is the energy crisis that arises from heavy dependence on nonrenewable energy sources. These resources are finite and contribute to environmental issues through burning [1]. Various options including biomass, wind energy, solar panels and hydropower, are being utilized to tackle the energy scarcity. Solar cells, considered as the optimal choice, provide clean and abundant energy, making a significant contribution to global efforts to achieve net-zero carbon emissions [2]. In the domain of solar cell technology, organic solar cells (OSCs) are regarded as cost-effective and environmentally sustainable. These OSCs exhibit various desirable

* Corresponding authors at: Institute of Chemistry, Khwaja Fareed University of Engineering & Information Technology, Rahim Yar Khan 64200, Pakistan.
** Corresponding authors.
E-mail addresses: muhammad.khalid@kfueit.edu.pk, khalid@iq.usp.br (M. Khalid), chen_ke@swmu.edu.cn (K. Chen).

https://doi.org/10.1016/j.jscs.2024.101903
Received 3 May 2024; Received in revised form 30 June 2024; Accepted 4 July 2024
Available online 7 July 2024

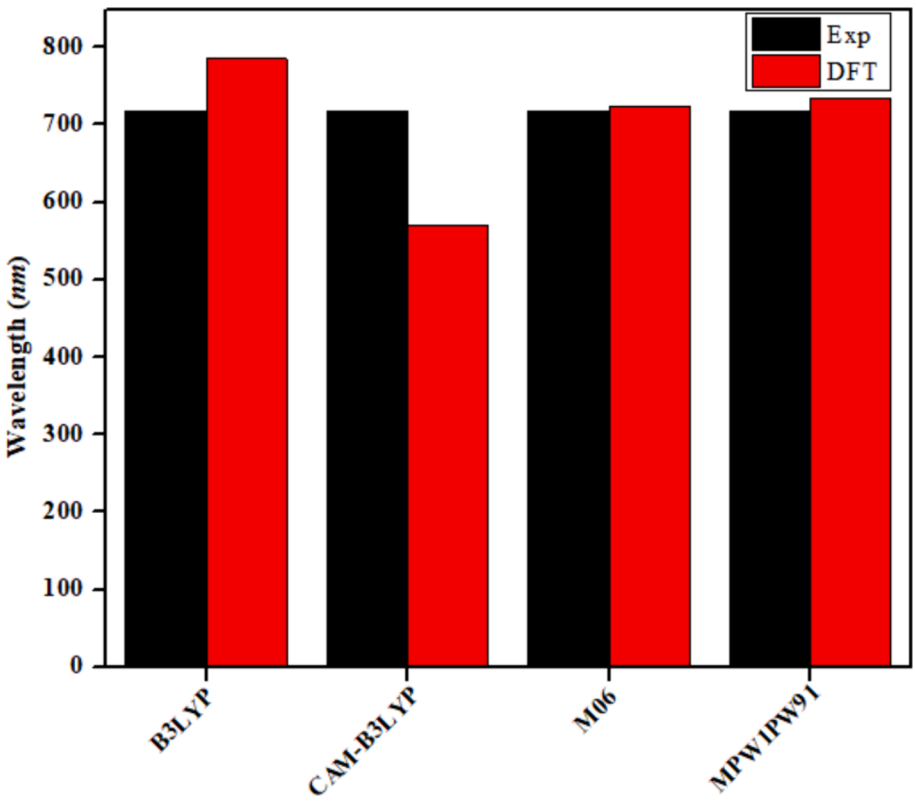

Fig. 1. A comparison between DFT based λ_{max} values at various functionals of **STMR** with its experimental λ_{max} value.

traits, including lightweight design, low manufacturing cost, adjustable electron energy levels, remarkable flexibility, and efficient power conversion [3]. Improvements in device parameters such as open-circuit voltage (V_{oc}), short-circuit current (J_{sc}), and fill factor (FF) is achieved through adjustments in the optoelectronics properties of organic materials [4]. Organic solar cells commonly utilize a bulk heterojunction (BHJ) architecture, which consists of a blended mixture of donor (D) and acceptor (A) materials. After absorbing light, the blended layers produce tightly bound excitons, which then separate into free carriers [5].

Fullerene and non-fullerene based photovoltaics (PVs) are the two pivotal classifications of organic solar cells (OSCs) [6]. Amongst different constituents in OSCs, acceptor materials have been crucial in dictating the device performance ratio, with fullerene derivatives yielding the highest PCE for nearly two decades. Moreover, blending organic solar cells with fullerene derivatives such as **$PC_{61}BM$** and **$PC_{71}BM$** etc. exhibits remarkable attributes, including low reorganization energies, elevated electron mobility, and isotropic charge transfer [7]. But, fullerene based acceptors also encounter certain drawbacks such as high production cost, restricted light absorption in the visible spectrum, and challenges in functionalization for energy level tuning, instabilities in morphology, and rapid degradation upon exposure to air. In answer to these constraints, scientists have been endeavoring to design and synthesize fullerene free OSCs materials [8]. Non-fullerene acceptors (NFAs), with their entirely conjugated structure, provide strong electron acceptance and consistent electron transport with aiding electron delocalization at donor–acceptor (D/A) interfaces [9]. The non-fullerene small molecule acceptors exhibit promising optical absorption properties, extending their absorbance into the infrared region[6]. Moreover, NFAs present various structural designs, including D-π-A, A1–π–A2–π–A1, D-A, A-π-D-π-A, and D-D-π-A. These configurations are commonly utilized in the development of effective organic solar cell (OSCs) materials [10]. The power conversion efficiency (PCE) of OSCs containing fused ring electron acceptors (FREAs) is rapidly boosted to over 18 %, indicating its promising prospects for commercialization. Currently, in molecular engineering, the primary focus of most studied FREAs is to improve light absorption properties, adjust energy levels, and charge transfer behavior through covalent modification [11].

Thiazole is an electron-deficient heteroatomic structure, owing to its nitrogen atom in the imine (C = N) moiety, and has been widely utilized to build organic semiconductor materials[12]. When compared to thiazole, chlorothiazole is expected to serve as a more electron-deficient component with deep lying HOMO energy level, capable of forming organic conjugated molecules. Recently, Han *et al,* designed and synthesized novel 4-chlorothiazole [13] based FREAs molecule for solar cell applications. These acceptor molecules achieved power conversion efficiency (PCE) of 11.10 %, with a favorable light absorption profile. Inspired by the findings of Han and colleagues, in this research new compounds **(STM1- STM6)** comprising A1–π–A2–π–A1 framework were designed by modifying the terminal acceptor units and thiophene π-spacer core with selenophene units of the reference molecule **(STMR)**. Substitution of selenophene units (π-spacer) in the molecular structure is driven by their ability to enhance charge carrier mobility through Se-Se intermolecular interactions and contribute to higher absorption properties than thiophene units[14]. Moreover, it has been noticed that the inclusion of selenophene units with benzothiophene based extended acceptors lowers the LUMO level while keeping the HOMO level unchanged, resulting in a substantial enhancement of both V_{oc} and J_{sc} in organic solar materials[15]. Various analyses have been conducted on designed compounds *via* DFT and TD-DFT techniques to explore the impact of structural tailoring on their electronic and photovoltaic behavior. This evaluation aimed to assess their suitability as effective materials for the production of high-performance solar devices.

2. Computational details

Gaussian 09 suite [16] was employed to calculate different DFT based analyses to comprehend the photovoltaic behavior of designed compounds (**STM1-STM6**). To identify the appropriate functional, we

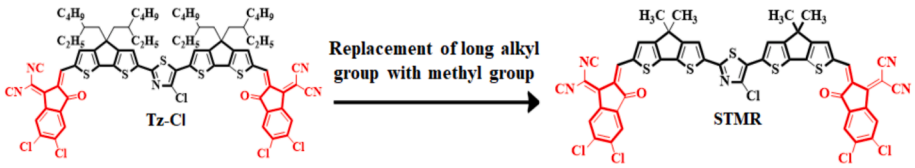

Fig. 2. Altering **Tz-Cl** into **STMR** by replacing long alkyl groups with methyl groups.

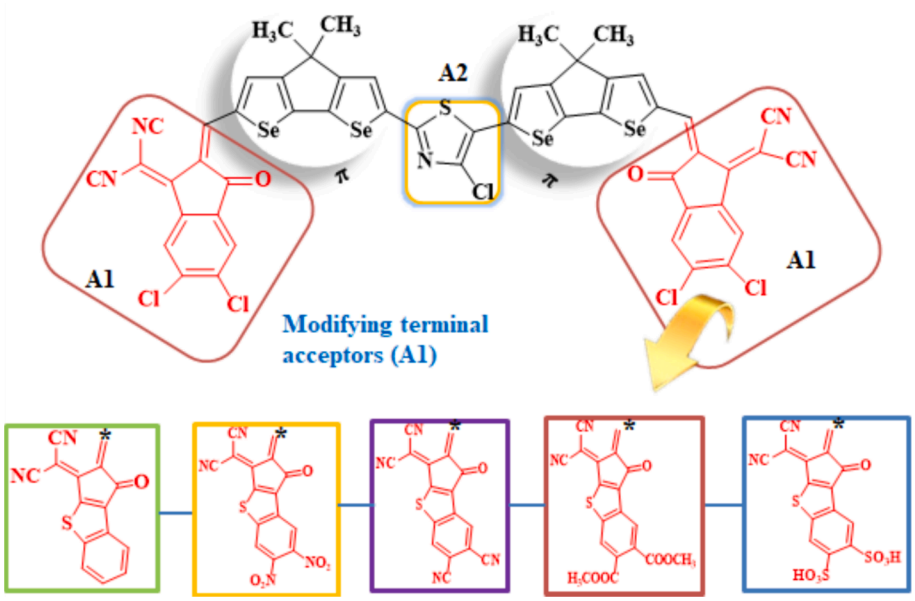

Fig. 3. Schematic representation of the designing of examined compounds **(STM1-STM6).**

conducted an evaluation comparing the TD-DFT calculated λ_{max} values of **STMR** with experimental data (718 *nm*) [13].For this purpose, reference compound **STMR** was optimized using four functionals including M06 [17], B3LYP [18], MPW1PW91 [19], and CAM-B3LYP [20]. Afterward, the optimized structure was subjected to UV–Vis analysis in chloroform solvent, yielding λ_{max} values of 723.193 *nm*, 784.958 *nm*, 733.895 *nm* and 570.856 *nm* for the mentioned functionals, respectively. The absorption spectra derived from DFT computations using M06 functional showed a close agreement with the experimental data (Fig. 1). Therefore, optimization of all designed systems was conducted at M06/6-311G(d,p) level. The absence of negative frequency indicated that all designed compounds are found at true minima. All the computational analysis were conducted at M06 level and 6-311G(d,p) basis set. The FMOs and UV–Vis analyses were executed using TD-DFT approach at M06 level and 6-311G(d,p) basis set. Moreover, DOS, TDM, V_{oc} E_b and electron hole analysis were also conducted to study optoelectronics and photophysical response of entitled chromophores. UV–Visible absorption investigation were performed in both gas and chloroform solvent at TD/M06 level and 6-311G(d,p) basis set. Various software such as Avogadro [21], GaussSum Version 2.0 [22], Multiwfn 3.7 [23], Chemcraft [24], PyMOlyze [25], and Origin [26] were used to extract data from output files, and data was organized into graphs and tables.

3. Results and discussion

The current study aims to investigate the photovoltaic behavior of organic chromophores categorized as NFAs. For this, **Tz-Cl** (A1–π–A2–π–A1) is chosen as a parent compound consisting of a chlorothiazole core flanked by two thiophene units (4,4-dimethyl-4H-cyclopental[1,2-b:4-b']dithiophene) serving as π-spacers. These thiophene rings are further connected to two identical terminal electron acceptor rings, specifically ((E)-2–2(2-ethylidene-1H-benzo[b]cyclopental[d]thiophen-3(2H)-ylidene) malononitrile). Initially, we designed **STMR** from **Tz-Cl** by replacing the side alkyl chain with methyl chain to alleviate computational expenses and steric hindrance as seen in Fig. 2. After that **STM-STM6** were developed by **STMR**, involving the substitution of thiophene rings of π spacer with selenophene moieties and terminal small acceptors with various extended acceptors units, illustrated in Fig. 3. The alteration aimed to enhance and investigate the influence of more effective utilization of selenophene and extended acceptor rings on electronic properties of OSCs materials. This theoretical research could significantly aid to understand the photovoltaic potential of these molecules before applying them in real-world uses. The optimized structures of mentioned compounds are shown in Fig. 4, and their corresponding Chemdraw structures are tabulated in Figure S1. However, the utilized acceptors moieties with their IUPAC names can be seen in Table S1. Moreover, cartesian coordinates of examined compounds are illustrated in Table S2–S8.

3.1. Electronic study

The study of frontier molecular orbitals (FMOs) is an effective method for exploring wide range optoelectronic properties *i.e.* electronic transitions, chemical stabilities, molecular reactivities and charge distribution in organic systems [27]. These parameters rely on the energy difference between the highest occupied molecular orbital (HOMO) and the lowest unoccupied molecular orbital (LUMO) [28]. According to valence band theory, the HOMO represents the valence band, while the LUMO signifies the conduction band [29]. The energy gap (ΔE) between the HOMO and LUMO significantly affects the absorption of photon, transfer of electrons, and the efficacy of solar cells. The molecules with smaller band gap leads to better performance, enabling electrons to shift rapidly from the HOMO to the LUMO state with minimal energy loss

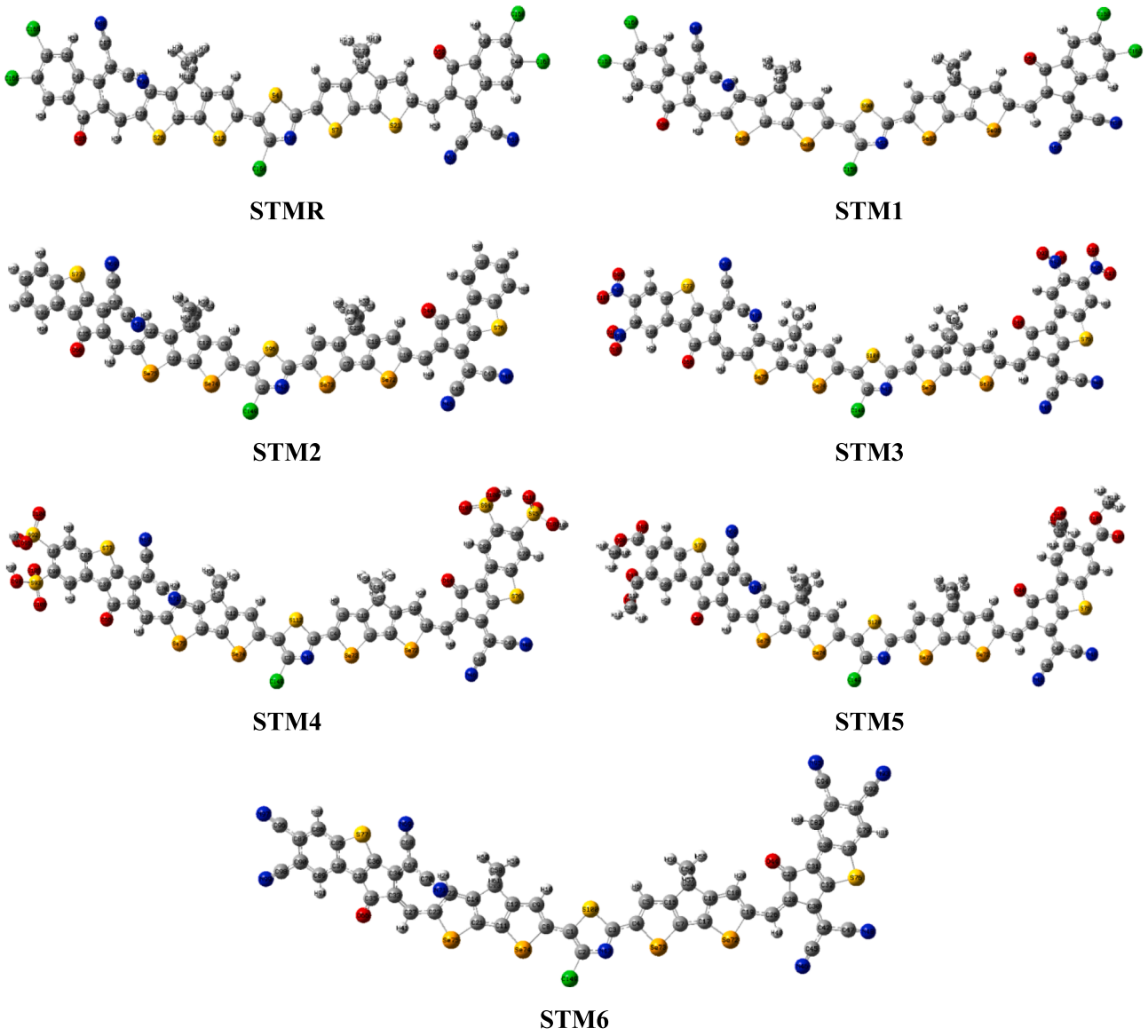

Fig. 4. Optimized structures of the examined chromophores (**STMR** and **STM1-STM6**).

Table 1
Energies of FMOs of **STMR** and **STM1-STM6**.

Chromophores	E_{HOMO}	E_{LUMO}	ΔE
STMR	−5.884	−3.610	2.274
STM1	−5.841	−3.649	2.192
STM2	−5.691	−3.454	2.237
STM3	−5.867	−3.789	2.078
STM4	−5.853	−3.749	2.104
STM5	−5.787	−3.617	2.170
STM6	−5.853	−3.745	2.108

$\Delta E = E_{\mathrm{LUMO}} - E_{\mathrm{HOMO}}$, units in *eV*.

[30,31]. Here, we explore how the electronic properties of engineered chromophores influence the behavior of photons. The information presented in Table 1 displays the orbital energies and band gap values for compounds **STMR** and **STM1-STM6** calculated at M06/6-311G (d,p) basis set and level. The surface diagrams of molecular orbitals for reference and the designed chromophores are presented in Fig. 5. Moreover, Table S24 presents the energy values, and Figure S2 depicts the pictorial representations of HOMO−1, HOMO−2, LUMO + 1, and LUMO + 2 for all the designed compounds.

The HOMO/LUMO energy values of **STMR-STM6** are calculated to be −5.884/−3.610–5.841/−3.649, 5.691/−3.454, −5.867/−3.789, −5.853/−3.749, −5.787/−3.617 and −5.853/−3.745 e*V*, respectively. The small terminal acceptors in **STMR** have been substituted with various powerful extended acceptor rings, and the thiophene rings of π-linker with more efficient selenophene rings. Consequently, a decrease in energy gap is evident across all the derivatives, as seen in Table 1. The computed band gap values between the HOMO and LUMO of **STMR-STM6** are 2.274, 2.192, 2.237, 2.078, 2.104, 2.170 and 2.108 *eV*, respectively. Among all designed compounds, **STM3** exhibits the narrowest band gap at 2.137 *eV*, which might be due the strong electron-accepting nature of nitro (–NO_2) groups attached at the terminal acceptors. NO_2 moiety is proficient at engaging in resonance by effectively transferring its unpaired electrons. Similarly, **STM4** with 2.104 *eV* energy gap, displays a smaller gap than **STM5** (2.170 *eV*), potentially attributed to the stronger electron-withdrawing effect of two oxygen atoms in the SO_3H group. Sulfonic acid group efficiently withdraws electronic density through inductive effects compared to the single oxygen atom in the CH_3COOH functionality. Similarly, **STM1** (2.192 *eV*) exhibits a smaller band gap than **STM2** (2.237 *eV*), owing to the presence of chlorobenzene functions at terminal acceptors that might likely

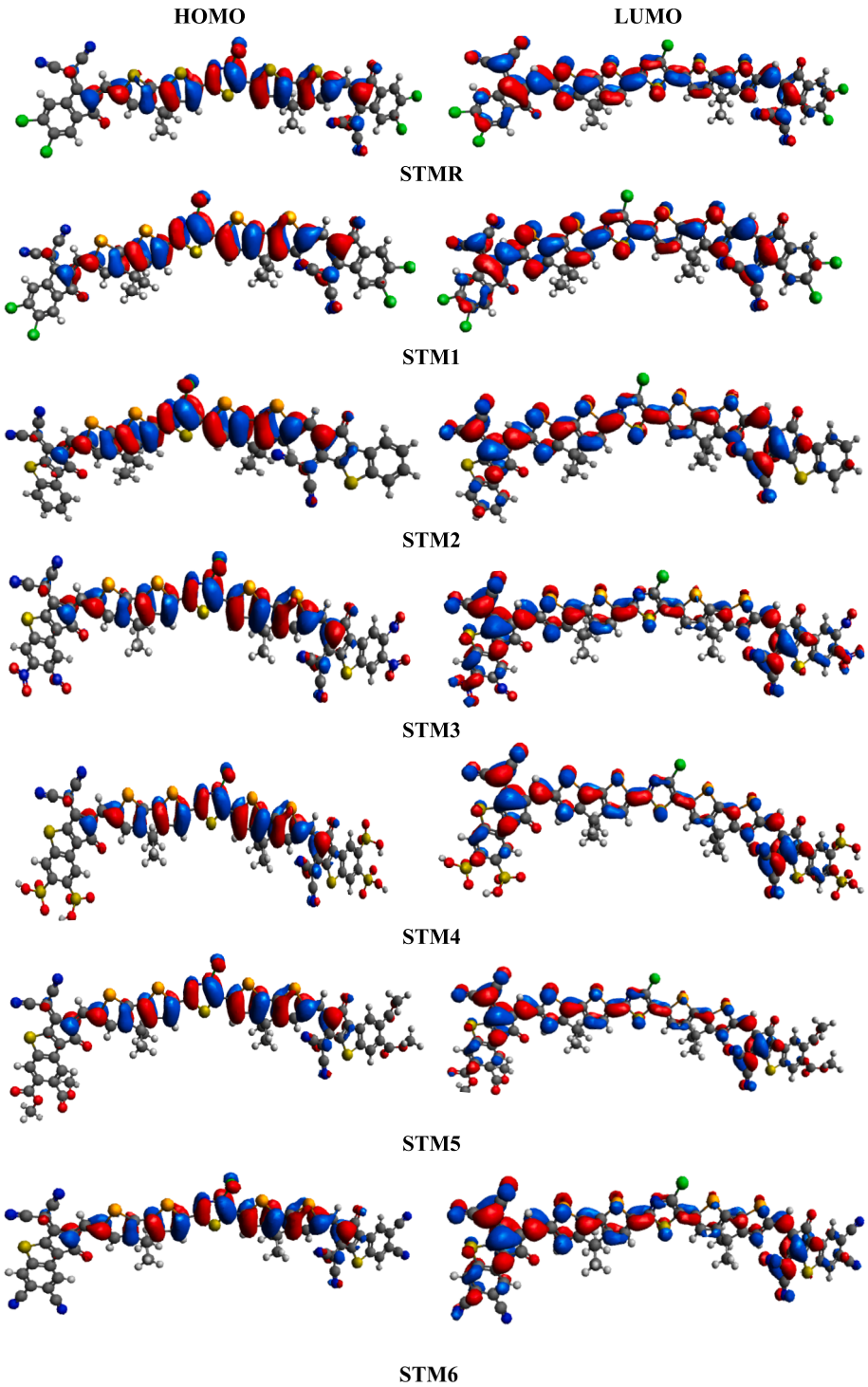

Fig. 5. HOMOs and LUMOs of **STMR** and **STM1-STM6**.

enhance the inductive effect more effectively than benzene. Overall, the increasing order of orbitals energy gaps of designed chromophores is as follows: **STM3** < **STM4** < **STM6** < **STM5** < **STM1** < **STM2** < **STMR**.

Surface diagrams of the FMOs aid in comprehending the charge transfer phenomena observed in **STMR** and **STM1- STM6**. Fig. 4 demonstrates that in the HOMO, the electronic density is majorly concentrated on whole molecule expect acceptor 1 and methyl moieties, whereas in the LUMO, charge density is located over entire compound except CH_3 groups. Overall, incorporating effective acceptor groups with strong electron-withdrawing moieties leads to a decreased orbital band gap, facilitating efficient charge transfer *via* π-spacer to the terminal acceptor portions, thus making them viable materials for organic solar cells (OSCs).

3.2. Global reactivity descriptors (GRDs)

The HOMO and LUMO band gap is a crucial factor for computing key reactivity descriptors of designed compounds. These variables include the electron affinity (*EA*) [32], ionization potential (*IP*) [33], chemical potential (μ) [34], electronegativity (X) [35], global hardness (η) [36],

Table 2
Computed GRDs of studied compounds (**STMR**) and (**STM1-STM6**).

Compounds	*IP*	*EA*	*X*	*η*	*μ*	*ω*	*σ*	ΔN_{max}
STMR	5.884	3.61	4.747	1.137	−4.747	9.909	0.439	4.175
STM1	5.841	3.649	4.745	1.096	−4.745	10.27	0.456	4.329
STM2	5.691	3.454	4.5725	1.118	−4.572	9.346	0.447	4.088
STM3	5.867	3.789	4.828	1.039	−4.828	11.21	0.481	4.646
STM4	5.853	3.479	4.666	1.187	−4.666	9.170	0.421	4.383
STM5	5.787	3.617	4.702	1.085	−4.702	10.18	0.460	4.333
STM6	5.853	3.745	4.799	1.054	−4.799	10.92	0.474	4.553

global softness **(*σ*)** eV^{-1}, all other units in *eV*.

electrophilicity index (*ω*) [37], and global softness (*σ*) [38].

The ionization potential and electron affinity of entitled compounds are calculated using following equations.

$$IP = -E_{\mathrm{HOMO}} \tag{1}$$

$$EA = -E_{\mathrm{LUMO}} \tag{2}$$

While other global reactivity descriptors are computed using the Koopmans's theorem [39]. The findings obtained from Eqs. (1)–(8) are presented in Table 2.

$$X = \frac{[IP + EA]}{2} \tag{3}$$

$$\eta = \frac{[IP - EA]}{2} \tag{4}$$

$$\mu = \frac{E_{\mathrm{HOMO}} + E_{\mathrm{LUMO}}}{2} \tag{5}$$

$$\sigma = \frac{1}{2\eta} \tag{6}$$

$$\omega = \frac{\mu^2}{2\eta} \tag{7}$$

ΔN_{max} indicates a compound's ability to absorb extra electrical charge from its surroundings, as determined by Eq. (8) [40].

$$\Delta N\mathrm{max} = -\mu/\eta \tag{8}$$

The electron-donating and electron-accepting nature of **STMR** and **STM1-STM6** can be determined through their electron affinity and ionization potential values. The ionization potential of designed compounds is observed to be lower compared to the reference compound **STMR** (5.884 *eV*). This suggests facile electron removal process with less amount of energy needed in designed chromophores than reference compound. The calculated descending order of ionization potential (*IP*) values is as follows: **STMR** (5.884 *eV*) > **STM3** (5.867 *eV*) > **STM4** (5.853 *eV*) > **STM6** (5.853 *eV*) > **STM1** (5.841 *eV*) > **STM5** (5.787 *eV*) > **STM2** (5.691 *eV*). The chemical potential serves as a valuable factor for elucidating the tendency of electrons to depart from an equilibrium state [41]. It demonstrates the following descending order for entitled compounds **STM3** (−4.828 *eV*) > **STM6** (−4.799 *eV*) > **STMR** (−4.747 *eV*) > **STM5** (−4.702 *eV*) > **STM1** (−4.745 *eV*) > **STM4** (−4.666 *eV*) > **STM2** (−4.572 *eV*). Similarly, global hardness and softness quantify the level of chemical reactivity and are reciprocally related to one another. A molecule characterized by a wider bandgap is considered to possess greater hardness, more stability, and less reactivity. Conversely, a compound featuring a narrower energy gap is regarded as softer, exhibiting more reactivity and less stability. The descending sequence of global softness is as follows: **STM3** (0.481 eV^{-1}) > **STM6** (0.474 eV^{-1}) > **STM1** (0.456 eV^{-1}) > **STM5** (0.460 eV^{-1}) > **STM2** (0.447 eV^{-1}) > **STMR** (0.439 eV^{-1}) > **STM4** (0.421 eV^{-1}). Furthermore, **STM3** exhibited the highest ΔN_{max}, recorded at 6.665 *eV*. All designed molecules exhibited the larger softness with lower hardness values thus regarded as polarizable and might possess advantageous photoelectric properties.

3.3. Optical properties

Analyzing the optical properties of the designed chromophores is conducted to assess their efficacy in organic solar cell applications. The absorption spectra of reference **(STMR)** and designed molecules **(STM1-STM6)** were computed both in chloroform solvent and in gaseous state *via* M06/6-311G (d,p) functional. The results pertaining with various

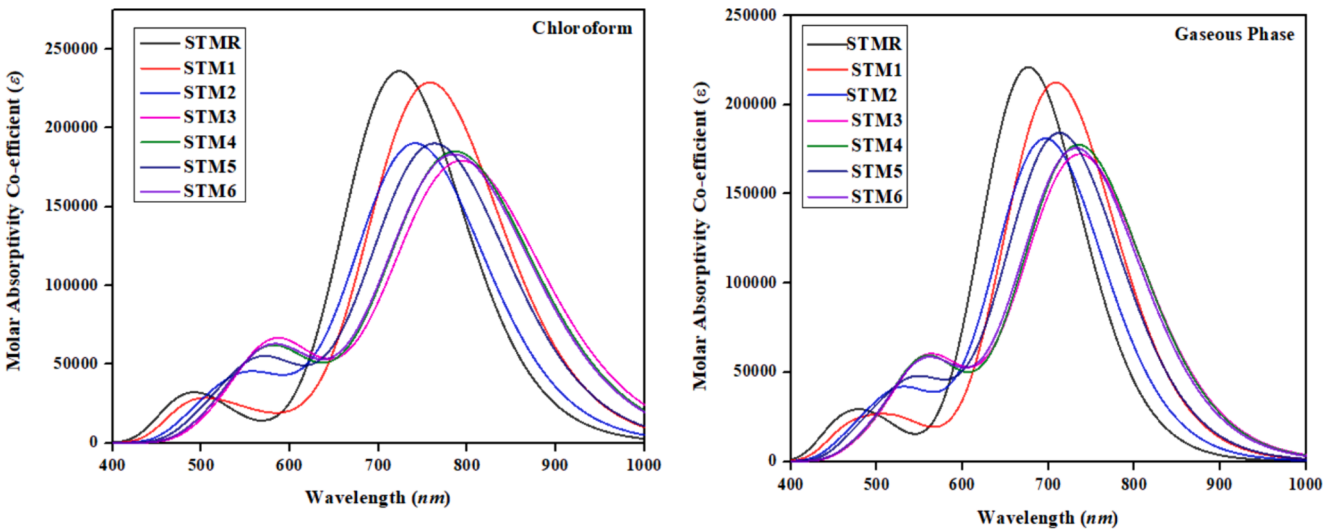

Fig. 6. The simulated absorption spectra of the studied compounds (**STMR-STM6**).

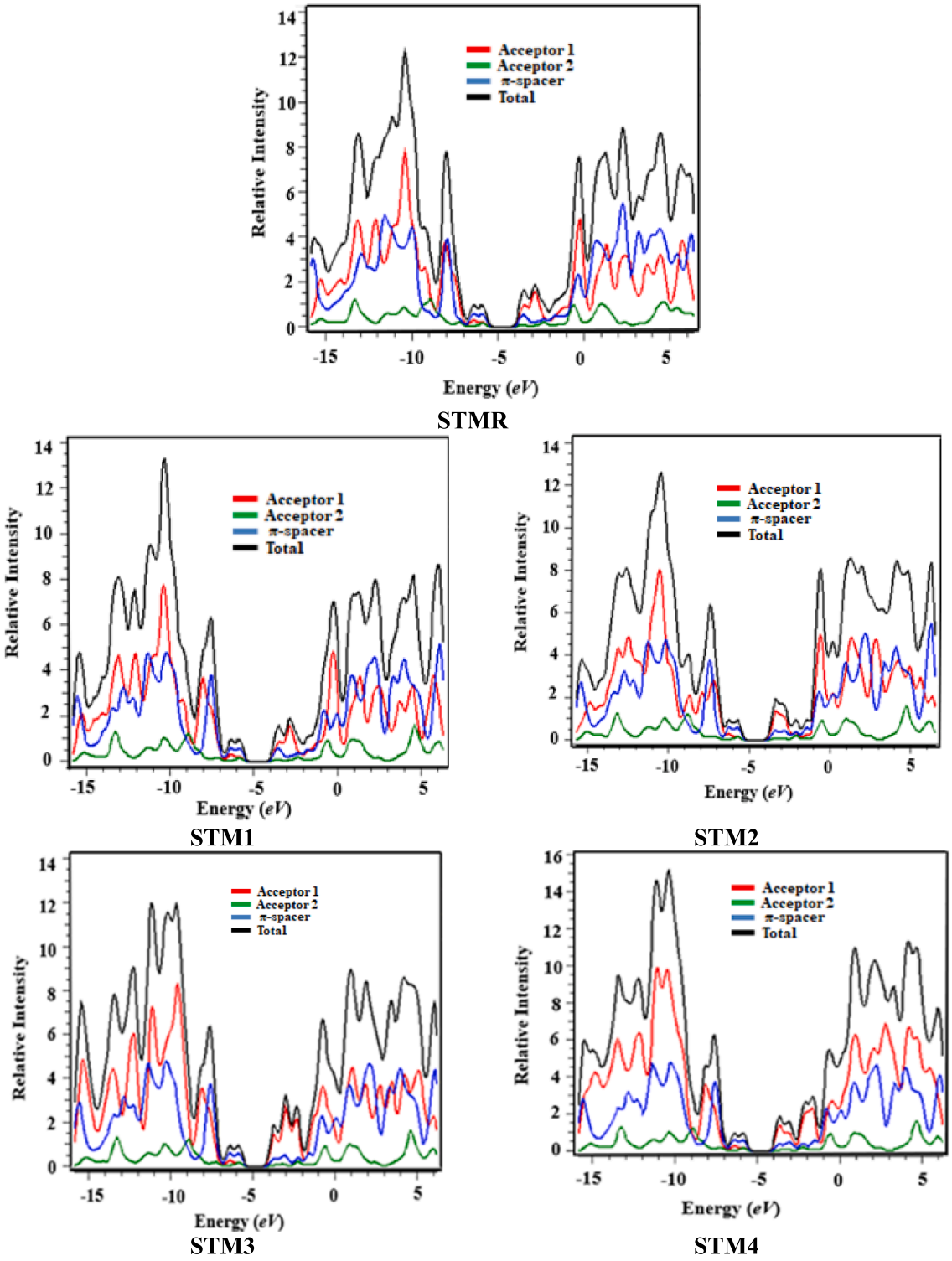

Fig. 7. DOS plots of the entitled chromophores (**STMR-STM6**).

optical parameters, such as absorption maxima (λ_{max}), oscillator strength (f_{os}), excitation energy (ΔE) along with concerned transitions are shown in Tables S8 and S9. Whereas, the six lowest transitions are detailed in Tables S10–S23.

All the studied compounds exhibited UV–Vis absorption in the range of 723.193–798.250 *nm* in chloroform and 676.290–738.793 *nm* in gaseous phase. However, designed chromophores **(STM1- STM6)** are observed with more significant bathochromic shift and lesser excitation energies values than reference (**STMR)** compound. This is due to the introduction of selenophene rings and extended acceptors with strong electron withdrawing groups that enhanced the conjugation [42,43]. Usually, a shift towards red in absorption spectra leads to enhanced power conversion efficiencies with improved electron mobility.

In the solvent phase, the absorption maxima (λ_{max}), values showed a greater red shift compared to the gaseous phase due to the solvent's influence. The polar medium is expected to stabilize the π–π* state by

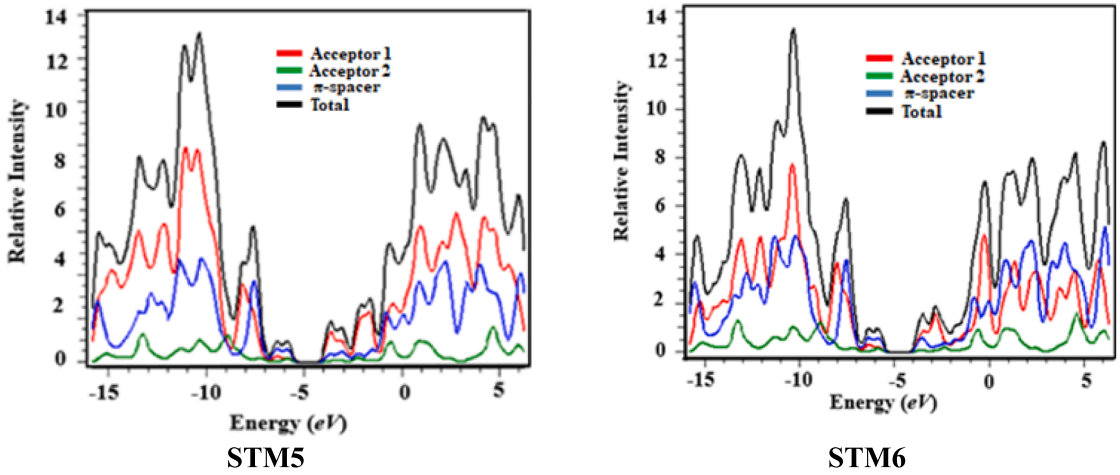

Fig. 7. (*continued*).

using suitable electronic states [44]. Among all the designed chromophores, **STM3** reveals the significant absorption maxima at 798.250 *nm* with the lowest value of excitation energy (*E*) at 1.553 *eV* and f_{os} of 2.372 with 90 % molecular orbital transition from H → L. This could be due to the existence of a potent electron-withdrawing acceptor groups, specifically 2-(2-methylene-6,7-dinitro-1-oxo-1,2-dihydro-benzo[b]cyclopenta[d]thiophene-3-ylidene)-malononitrile, at the terminals. A low excitation energy value and a narrower energy gap enhance charge transport, making the transition from H → L easier and thereby increasing PCE. The declining wavelength order of all the examined compounds in chloroform solvent is observed in *nm* as follows: **STM3** (798.250) > **STM4** (790.060) > **STM6** (789.055) > **STM5** (766.091) > **STM1** (757.803) > **STM2** (744.650) **STMR** (723.193). In the gaseous phase same decreasing pattern of λ_{max} (*nm*) is evident as follows: **STM3** (738.793) > **STM4** (736.204) > **STM6** (734.243) > **STM1** (708.441) > **STM5** (714.936) > **STM2** (697.952) > **STMR** (676.290). The simulated absorption spectra in both chloroform and gas phase of all the designed molecules is given in Fig. 6.

3.4. Density of state (DOS)

Density of states (DOS) denotes the number of available electronic states at a specific energy level. In terms of energy levels, a higher density of state value indicates multitude unoccupied states [45]. Moreover, this investigation aims to identify the role of each fragment of molecule in generating distinct energy levels, mainly the HOMO and LUMO. Thus, it helps to confirm the outcomes attained from FMO analysis and percentage impact of HOMO and LUMO on the charge densities. DOS analysis for the entitled compounds was conducted at M06/6-311G (d,p) functional, with graphical representations provided in Fig. 7. In this study, **STMR** and **STM1-STM6** were segmented into three components: A1 (end capped acceptors), π-linker, and A2 (4-chlorothiazole) structured as A1–π–A2–π–A1. The negative values along the x-axis illustrate the HOMO (valence band), while positive values indicate the LUMO (conduction band). The separation between these conduction and valence bands denotes the band gap. The concentration of charge on HOMO and LUMO of acceptor 1, acceptor 2, and the π-linker is represented by the colors red, green, and blue, respectively, as depicted in Fig. 5. The black band represents the combined electronic contribution covering the entirety of the molecule.

Table S25 manifested that, the terminal acceptors (A1) show the charge distribution pattern with 21.5, 21.6, 18.1, 19.7, 19.8, 18.9 and 19.5 % to HOMO while 52.2, 47.7, 59.0, 70.1, 67.2, 64.0 and 67.3 % to LUMO for **STMR-STM6**, respectively. Similarly, the *π*-spacer contributes charge distribution pattern of 59.6, 60.3, 63.5, 61.6, 61.5, 62.5 and 61.8 % charge towards HOMOs, while 38.6, 42.5, 33.1, 24.8, 27.1, 29.5 and 19.5 % to LUMOs in all the examined compounds, respectively. Likewise, A2 exhibited electron contributions to HOMO as follows: 18.9, 18.1, 18.4, 18.7, 18.7, 18.6 and 18.7 % while contributing 9.2, 9.8, 7.9, 5.1, 5.7, 6.5 and 5.7 % to LUMO for all the studied compounds. The introduction of strong withdrawing acceptors with selenophene rings impacts the charge density around HOMO and LUMO, as clearly shown in above pictographs. These observations confirm that modifying peripheral acceptor motifs enables various types of electronic transmission.

3.5. Transition density matrix (TDM) analysis

Transition density matrix analysis serves as a valuable tool to understand nature of transitions between two quantum states, often involving a molecule shifting from its ground state to an excited state. Furthermore, it aids to examine the interactions between acceptor and donor components, hole and electron overlapping, and degree of internal charge transfer [46]. The evaluation of these parameters helps to determine the performance of OSCs. All the designed chromophores **(STMR- STM6)** are analyzed at first excitation state (S_1) using M06/6-311G(d,p) basis set and level (Fig. 8). In this research, significance of hydrogen atoms has been ignored as they show minimal influence on charge transition. To conduct this investigation we divided our compounds into three distinct segments: the terminal acceptor units (A1), the central core acceptor unit (A2), and π-linker, as outlined in Scheme 1. This analysis provides a three-dimensional heat map with distinct color variations, as indicated by the blue region.

TDM heat maps depicted a prominent diagonal transfer of charge density from the central core (A2) through the π-bridge to terminal units (A1) in all the studied compounds. Furthermore, the creation of electron-hole pairs and the coherence of charges also seemed to spread in a non-diagonal manner. The above shown heat maps also supported DOS and FMO findings where same electron transfer trend was observed. It is noted from graphs that some of the electron coherence is found on the π-linker and A1, while most of it is concentrated on acceptor 2 without trapping any charge.

3.6. Exciton binding energy (E_b)

The binding energy (E_b) of holes and electron plays a crucial role to determine the molecular optoelectronic properties [47]. In OSCs materials, it signifies the energy needed to separate an electron-hole (exciton) pair formed upon photon absorption. The coulombic forces between holes and electrons are calculated by evaluating binding energy. The substitution of extended end-capped acceptors aids in decreasing coulombic forces, facilitating easier dissociation thereafter. The binding

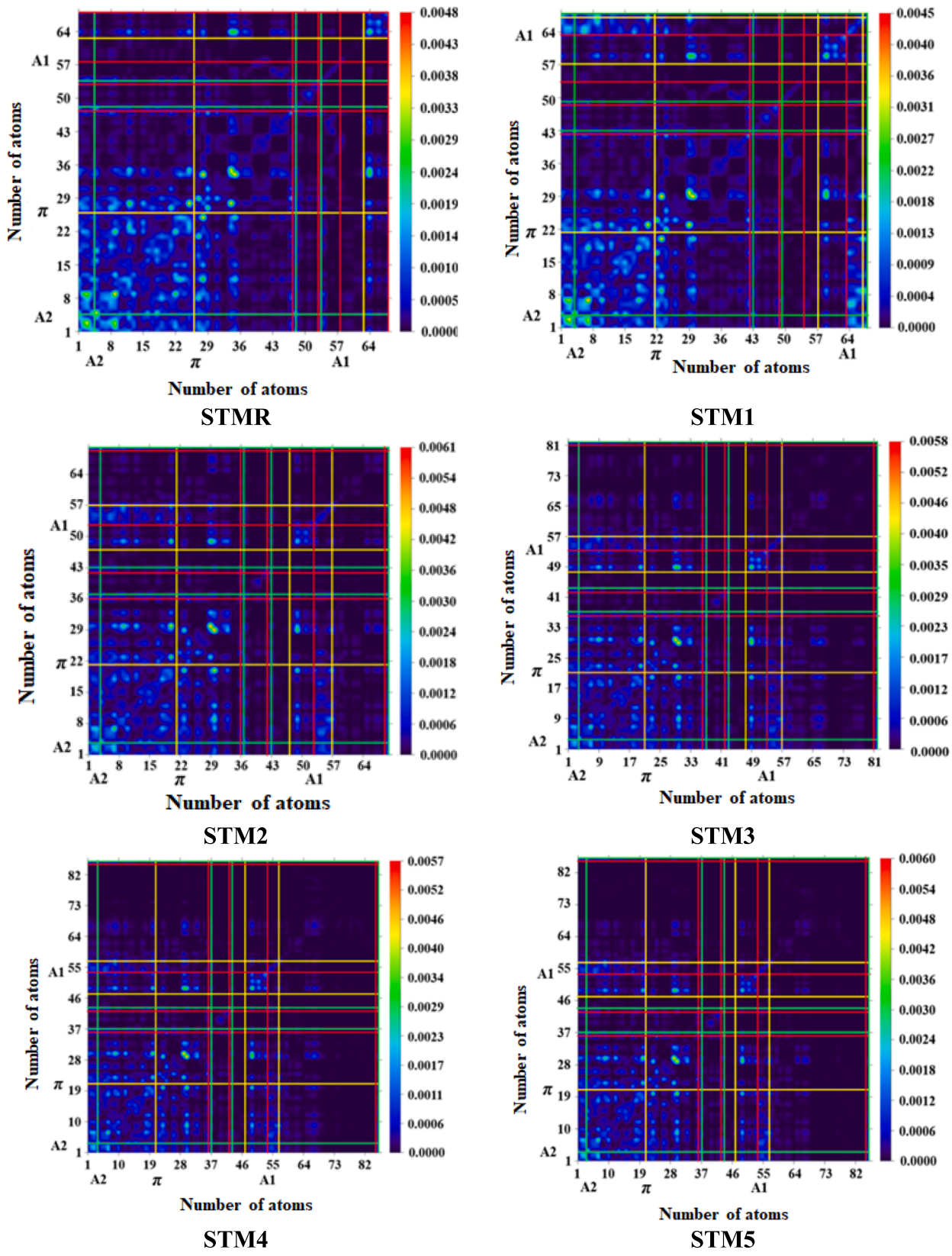

Fig. 8. TDM graphs of **STMR-STM6** at first excitation state.

energy is directly related with columbic forces. As it decreases, columbic interaction also decreases, resulting in increased exciton dissociation and improved charge mobility in the excited states. The exciton binding energy for **STMR** and **STM1-STM6** chromophores are calculated using below Equation.

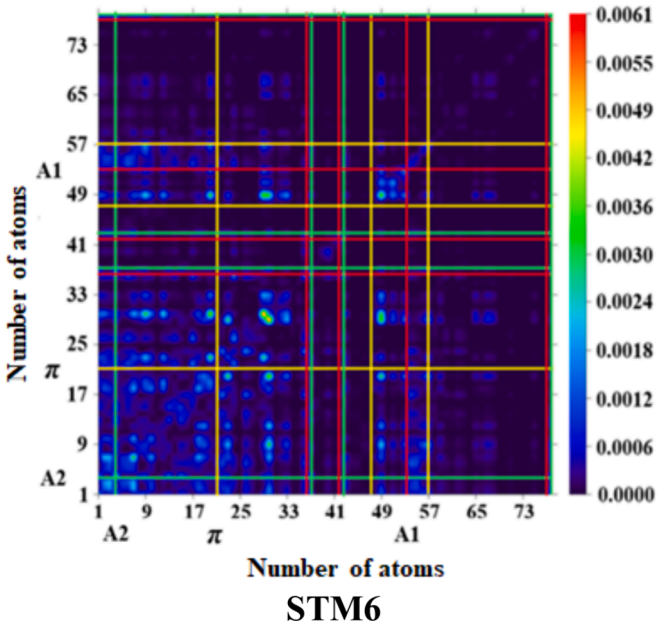

Fig. 8. (*continued*).

Table 3
The exciton cohesion energies of **STMR** and **STM1-STM6** compounds.

Compounds	$E_{H\text{-}L}$	E_{opt}	E_b
STMR	2.274	1.714	0.560
STM1	2.192	1.636	0.556
STM2	2.237	1.665	0.572
STM3	2.078	1.553	0.525
STM4	2.104	1.569	0.535
STM5	2.170	1.618	0.552
STM6	2.108	1.571	0.537

Units in *eV*.

$$E_b = E_{H\text{-}L} - E_{opt} \quad (9)$$

Here, $E_{H\text{-}L}$ represents the band gap between HOMO and LUMO. E_{opt} refers to the minimum energy required for the first excitation from the ground state (S_0) to the first singlet excited state (S_1), involving electron hole pair.

Table 3 summarized a comparable trend to $E_{H\text{-}L}$ is observed in E_{opt}. Moreover, the values of E_b for **STMR** and **STM1-STM6** are computed to be 0.560, 0.556, 0.572, 0.525, 0.535, 0.552 and 0.537 *eV,* respectively. **STM3** exhibited the lowest exciton binding energy value among all designed compounds, indicating its higher rate of exciton separation and potential to significantly enhance overall current charge density. The exciton cohesion energies of examined compounds decrease as: **STM2** > **STMR** > **STM1** > **STM5** > **STM6** > **STM4** > **STM3**. These chromophores might prove as promising candidates for non-fullerene based organic solar cells due to their ability to generate maximum voltage. In our study, the calculated exciton binding energies are reasonable low. Therefore, it is expected that exciton rates for the predicted materials may be significant.

3.7. Open circuit voltage (V_{oc})

Open circuit voltage (V_{oc}) serves as a key indicator to analyze the efficiency and working mechanics of OSCs[48]. In essence, higher V_{oc} values correspond to greater OSCs performance as it represents the maximum achievable current from the optical material at zero voltage. It depends upon E_{HOMO} and E_{LUMO} of donor polymer and acceptor molecule, respectively, playing a crucial role in transferring charge from the donor polymer's HOMOs to the acceptor material's LUMOs. Achieving higher V_{oc} in organic solar cells is possible when the LUMO level of acceptor possess less energy compared to HOMO level of donor polymer[49]. In this study, we relate the HOMO level of well-known donor polymer **PBDB-T**[50] with the LUMO level of all our designed compounds and −2.328 *eV* is computed E_{LUMO} value for the donor polymer. Theoretically computed V_{oc} values for all examined chromophores were calculated using Eq. (10) [51], introduced by Sharber and colleagues and the results are outlined in Fig. 9 and Table 4. The open circuit voltage (V_{oc}) results were found with overestimated values, might be due to purly theoretical approach.

$$V_{oc} = (|E^{D}_{HOMO}| - |E^{A}_{LUMO}|) - 0.3 \quad (10)$$

$E^{(D)}_{HOMO}$ represents HOMOs level of donor and $E^{(A)}_{LUMO}$ signifies the LUMOs level of acceptor. The empirical coefficient 0.3 *V* accounts for losses during charge transport to the electrodes.

The band gap values of HOMOs and LUMOs of donor and acceptor complexes observed as 1.791, 1.752, 1.947, 1.612, 1.922, 1.784, 1.656 V for **STMR-STM6,** respectively (Table 4). This indicated that **PBDB-T: STM2** and **PBDB-T: STM4** complexes exhibit the largest band gap value than other complexes. V_{oc} of **STMR** corresponding to $HOMO_{donor}$-$LUMO_{PBDBT}$ has been calculated as 1.491 *V*. The calculated V_{oc} values for **STMR-STM6** chromophores are: 1.491, 1.452, 1.647, 1.312, 1.622, 1.484, 1.356 *V*, respectively. All the designed compounds showed comparable V_{oc} values to reference compound. Its decreasing trend for all designed compounds is as follows: **STM2 < STM4 < STMR < STM5 < STM1 < STM6 < STM3.** As mentioned earlier, the open-circuit voltage is influenced by the energy levels of HOMO of the donor and LUMO of the acceptor materials. A lower LUMO originating from the acceptor leads to a higher V_{oc} value and enhances the optoelectronic characteristics. The Fig. 9 illustrates that the LUMO energy level of **PBDB-T** is situated at a higher energy level compared to the LUMO energy level of the acceptor chromophores. This facilitates the transportation of electrons from the donor to the acceptor segments, which increases the optoelectronic features of all the examined compounds.

3.8. Hole-electron analysis

Electron hole analysis offer understanding of behavior of charge carriers and excitations in photovoltaic materials **(STMR-STM6)** [52]. Electron excitation analysis was conducted using Multiwfn 3.8. Fig. 10

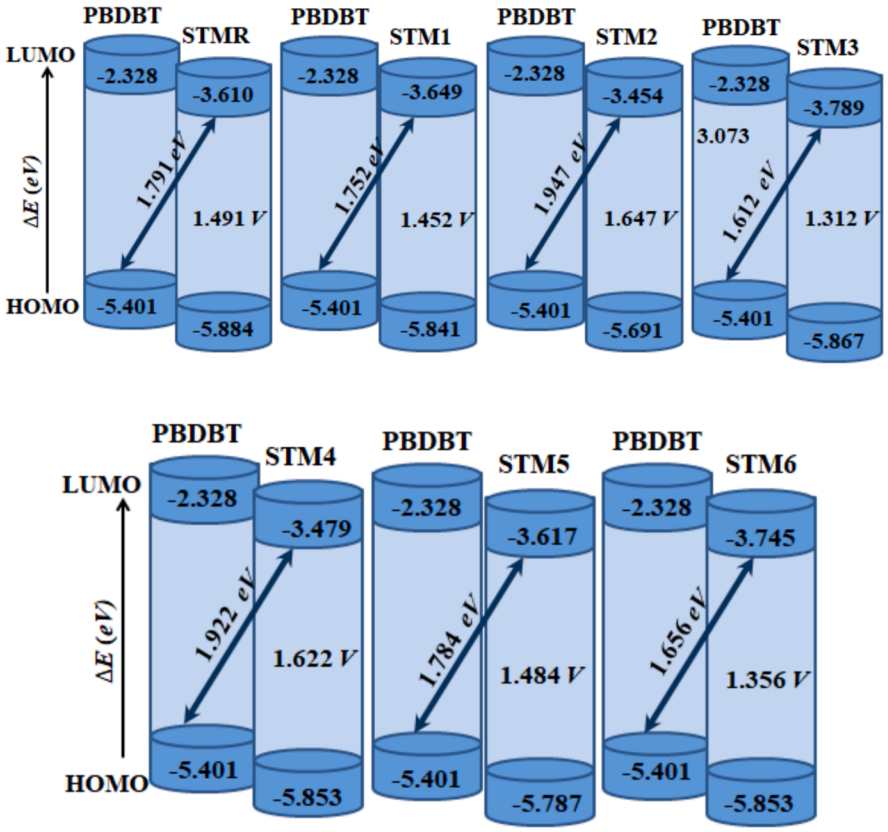

Fig. 9. V_{oc} diagrams of entitled chromophores with **PBDB-T**.

Table 4
The calculated V_{OC} values of designed compounds **(STMR-STM6).**

Compounds	V_{OC} (V)	Δ E (eV)
STMR	1.491	1.791
STM1	1.452	1.752
STM2	1.647	1.947
STM3	1.312	1.612
STM4	1.622	1.922
STM5	1.484	1.784
STM6	1.356	1.656

illustrates that in **STMR**, hole is generated at sulphur atom (S21) of thiophene ring of π-spacer. Simultaneously, a notable electronic cloud is evident at C27 of the π-bridge. This could be due to the strong electron-withdrawing capability of the sulfur group. It is evident that a positive charge (hole) is generated in different atoms of π-inkers, progressing towards the acceptor region that shows effective charge transfer from the π-bridge to the acceptor group in all the designed compounds **(STM1-STM6)**.

For **STM1** and **STM2** the highest hole intensity is detected at C17 (π-spacer) and electronic density at C22 of selenophene for **STM1** and, C25 (π-linker), C28 and C38 of terminal acceptors for **STM2**, respectively. Similarly, **STM3** contain thick hole density at C9 of π-spacer and electron density at C38 of extended terminal acceptors. The highest hole density for **STM4**, **STM5**, **STM6** is found thick at C9 and C7 atoms of π-spacer (selenophene), while electronic density is found dense at C28 and C38 of Acceptor 1 and C25 in 5,5-dimethylcyclopenta-1,3-diene moiety of π-linker.

Thus, Fig. 9, shows that high intensity holes are observed at various atoms of the π-linker, with charge transfer occurring at the acceptor region. These carbon atoms are connected to the terminal electron withdrawing groups, facilitating efficient intramolecular charge transfer (ICT) in all the derivatives (**STM1-STM6).** All the chromophores are observed with substantial electron and hole clouds at different portion of molecules. However, among all the studied compounds **STM2** seems to be a best candidate as an electron rich material.

4. Conclusion

In a nutshell, the chlorothiazole core based chromophores with A1–π–A2–π–A1 architecture have been designed *via* structural modulation to make efficient photovoltaic materials. Different types of extended benzothiophene based electron-withdrawing groups and highly polarizable selenophene units have been introduced to attain greater red-shift with reduced energy gap. A reduction in the band gaps (ΔE) in the range of 2.399–2.064 *eV*, with a larger bathochromic shift in span of 655.480–728.376 *nm* and lower binding energies (E_b = 0.508–0.362 *eV*) are obtained. These results indicate a higher exciton dissociation rate and significant charge transfer from HOMO to LUMO, which is further confirmed by TDM and DOS analyses. Among all the compounds studied, **STM3** demonstrated the remarkable optoelectronic properties, with a band gap of 2.078 *eV*, a bathochromic shift reaching 798.250 *nm*, and a lower value of exciton binding energy of 0.525 *eV*. A notable V_{oc} value is observed across all designed materials when blended with **PBDB-T** polymer. Its decreasing order for all the examined compounds is noticed as: **STM2** (1.647 *V*) < **STM4** (1.622 *V*) < **STMR** (1.491 *V*) < **STM5** (1.484 *V*) < **STM1** (1.452 *V*) < **STM6** (1.356) < **STM3** (1.312 V). A significant V_{oc} value is observed for **STM2** (1.647 *V*) among all modulated compounds. Moreover, electron hole analysis was also conducted and **STM2** is observed as best compound with maximum electron hole creation. All the results indicate that the designed chromophores hold potential to use as OSCs material due to their improved photovoltaic properties.

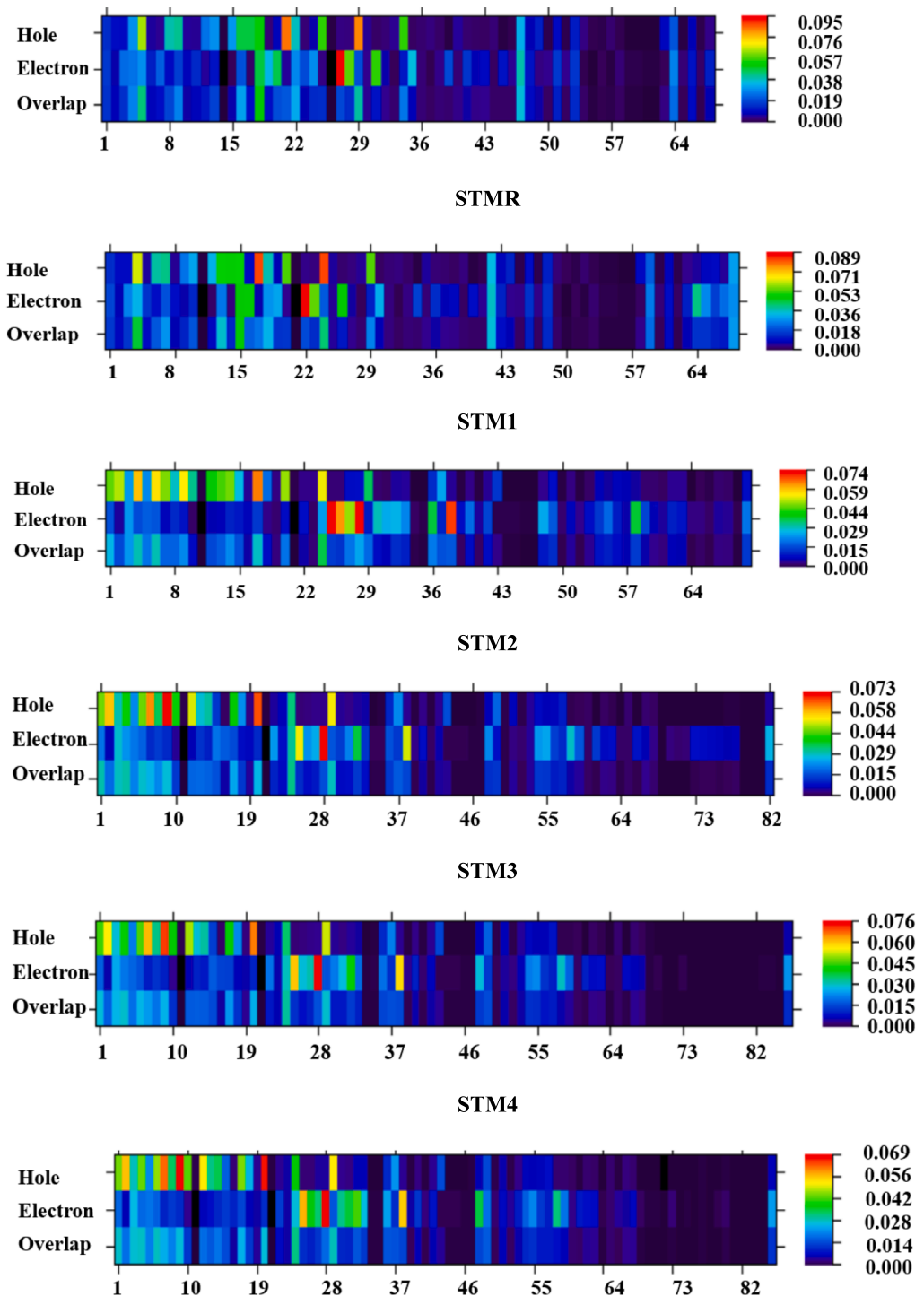

Fig. 10. Electron Hole analysis of the studied chromophores **(STMR-STM6)**.

5. Availability of data and materials

All data generated or analyzed during this study are included in this published article and its supplementary information files.

CRediT authorship contribution statement

Muhammad Khalid: Writing – review & editing, Investigation, Formal analysis, Data curation, Conceptualization. **Sadia Jamal:** Writing – original draft, Visualization, Validation, Formal analysis, Data curation. **Ataualpa Albert Carmo Braga:** Visualization, Validation, Supervision, Software, Resources. **Muhammad Haroon:** Writing – review & editing, Investigation, Formal analysis, Data curation, Conceptualization. **Rajeh Alotaibi:** Writing – review & editing, Validation, Funding acquisition, Formal analysis, Data curation. **Ke Chen:** Writing – review & editing, Visualization, Funding acquisition, Formal analysis, Data curation.

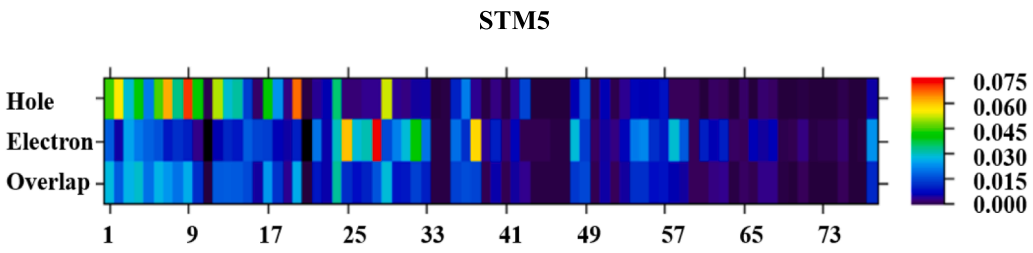

Fig. 10. (*continued*).

Declaration of Competing Interest

The authors declare that they have no known competing financial interests or personal relationships that could have appeared to influence the work reported in this paper.

Acknowledgments

Dr. Muhammad Khalid gratefully acknowledges the financial support of HEC Pakistan (project no. 20-14703/NRPU/R&D/HEC/2021). A. A.C.B. (grants 2011/07895-8, 2015/01491-3, and 2014/25770-6) is highly thankful to Fundação de Amparo à Pesquisa do Estado de São Paulo for the cooperation and financial assistance. A.A.C.B. (grant 312550/2020-0) also thanks to the Brazilian National Research Council (CNPq) for financial support and fellowships. The authors thank Researchers Supporting Project number (RSPD2024R644), King Saud University, Riyadh, Saudi Arabia. K.C. acknowledges the support from the doctoral research fund of the Affiliated Hospital of Southwest Medical University.

Appendix A. Supplementary data

Supplementary data to this article can be found online at https://doi.org/10.1016/j.jscs.2024.101903.

References

[1] G. Li, R. Zhu, Y. Yang, Polymer Solar Cells. Nature Photonics. 6 (2012) 153–161.
[2] B. Energy, Renewable energy sources, Ergon Energy, 2015.
[3] L. Lu, T. Zheng, Q. Wu, et al., Recent advances in bulk heterojunction polymer solar cells, Chemical Reviews. 115 (2015) 12666–12731.
[4] M.-H. Jao, H.-C. Liao, W.-F. Su, Achieving a high fill factor for organic solar cells, Journal of Materials Chemistry a. 4 (2016) 5784–5801.
[5] J. Roncali, Molecular bulk heterojunctions: an emerging approach to organic solar cells, Accounts of Chemical Research. 42 (2009) 1719–1730.
[6] C. Yan, S. Barlow, Z. Wang, et al., Non-fullerene acceptors for organic solar cells, Nature Reviews Materials. 3 (2018) 1–19.
[7] A. Armin, W. Li, O.J. Sandberg, et al., A history and perspective of non-fullerene electron acceptors for organic solar cells, Advanced Energy Materials. 11 (2021) 2003570.
[8] Y. Lin, X. Zhan, Non-fullerene acceptors for organic photovoltaics: an emerging horizon, Materials Horizons. 1 (2014) 470–488.
[9] J. Chen, Y. Chen, L.-W. Feng, et al., Hole (donor) and electron (acceptor) transporting organic semiconductors for bulk-heterojunction solar cells, EnergyChem. 2 (2020) 100042.
[10] M. Wielopolski, J.-H. Kim, Y.-S. Jung, et al., Position-dependent extension of π-conjugation in D-π-A dye sensitizers and the impact on the charge-transfer properties, The Journal of Physical Chemistry c. 117 (2013) 13805–13815.
[11] J. Wang, X. Zhan, Fused-ring electron acceptors for photovoltaics and beyond, Accounts of Chemical Research. 54 (2020) 132–143.
[12] M. Ji, C. Dong, Q. Guo, et al., Recent Advances in Organic Photovoltaic Materials Based on Thiazole-Containing Heterocycles, Macromolecular Rapid Communications. 44 (2023) 2300102.
[13] Z. Han, C. Li, X. Gu, et al., Combination of S··· N and S··· Cl Noncovalently Conformational Locks for Constructing High-Planarity and Low-Cost Nonfused-Ring Electron Acceptors, Chinese Journal of Chemistry. 41 (2023) 1797–1802.
[14] V. Cuesta, M. Vartanian, P. Malhotra, et al., Increase in efficiency on using selenophene instead of thiophene in π-bridges for D-π-DPP-π-D organic solar cells, Journal of Materials Chemistry a. 7 (2019) 11886–11894.
[15] B. Fan, F. Lin, X. Wu, et al., Selenium-containing organic photovoltaic materials, Accounts of Chemical Research. 54 (2021) 3906–3916.
[16] Frisch, M. J.; Trucks, G. W.; Schlegel, H. B, et al., 2009. Gaussian 09, Revision d. 01, Gaussian. Inc, Wallingford CT. 201.
[17] V.S. Bryantsev, M.S. Diallo, A.C. Van Duin, et al., Evaluation of B3LYP, X3LYP, and M06-class density functionals for predicting the binding energies of neutral, protonated, and deprotonated water clusters, Journal of Chemical Theory and Computation. 5 (2009) 1016–1026.
[18] B. Civalleri, C.M. Zicovich-Wilson, L. Valenzano, et al., B3LYP augmented with an empirical dispersion term (B3LYP-D*) as applied to molecular crystals, CrystEngComm. 10 (2008) 405–410.
[19] C. Adamo, V. Barone, Exchange functionals with improved long-range behavior and adiabatic connection methods without adjustable parameters: The m PW and m PW1PW models, The Journal of Chemical Physics. 108 (1998) 664–675.
[20] T. Yanai, D.P. Tew, N.C. Handy, A new hybrid exchange–correlation functional using the Coulomb-attenuating method (CAM-B3LYP), Chemical Physics Letters. 393 (2004) 51–57.
[21] M.D. Hanwell, D.E. Curtis, D.C. Lonie, et al., Avogadro: an advanced semantic chemical editor, visualization, and analysis platform, Journal of Cheminformatics. 4 (2012) 1–17.
[22] O'Boyle, N., GaussSum, Version 2.0. 5, 2007.
[23] T. Lu, F. Chen, Multiwfn: A multifunctional wavefunction analyzer, Journal of Computational Chemistry. 33 (2012) 580–592.
[24] Zhurko, G. and D. Zhurko, 2009. ChemCraft, version 1.6. URL: http://www. chemcraftprog. com.
[25] N.M. O'boyle, A.L. Tenderholt, K.M. Langner, Cclib: a library for package-independent computational chemistry algorithms, Journal of Computational Chemistry. 29 (2008) 839–845.
[26] K.J. Stevenson, Review of originpro 8.5, Journal of the American Chemical Society. 133 (2011) 5621.
[27] S.U. Rehman, A. Samad, M. Saeed, et al., Computational insight of ZrS2/graphene heterobilayer as an efficient anode material, Applied Surface Science. 551 (2021) 149304.
[28] S.P. Bremner, C. Yi, I. Almansouri, et al., Optimum band gap combinations to make best use of new photovoltaic materials, Solar Energy. 135 (2016) 750–757.
[29] J. Wang, S. Cong, S. Wen, et al., A rational design for dye sensitizer: density functional theory study on the electronic absorption spectra of organoimido-substituted hexamolybdates, The Journal of Physical Chemistry c. 117 (2013) 2245–2251.
[30] L. Yang, J.-K. Feng, A.-M. Ren, Theoretical study on electronic structure and optical properties of phenothiazine-containing conjugated oligomers and polymers, The Journal of Organic Chemistry. 70 (2005) 5987–5996.
[31] F. Kandemirli, S. Sagdinc, Theoretical study of corrosion inhibition of amides and thiosemicarbazones, Corrosion Science. 49 (2007) 2118–2130.
[32] M. Srnec, E.I. Solomon, Frontier molecular orbital contributions to chlorination versus hydroxylation selectivity in the non-heme iron halogenase SyrB2, Journal of the American Chemical Society. 139 (2017) 2396–2407.
[33] R.G. Parr, W. Yang, Density functional approach to the frontier-electron theory of chemical reactivity, Journal of the American Chemical Society. 106 (1984) 4049–4050.
[34] P. Politzer, D.G. Truhlar, Chemical applications of atomic and molecular electrostatic potentials: reactivity, structure, scattering, and energetics of organic, inorganic, and biological systems, Springer Science & Business Media, 2013.
[35] R.G. Parr, R.G. Pearson, Absolute hardness: companion parameter to absolute electronegativity, Journal of the American Chemical Society. 105 (1983) 7512–7516.
[36] R.G. Pearson, Absolute electronegativity and absolute hardness of Lewis acids and bases, Journal of the American Chemical Society. 107 (1985) 6801–6806.
[37] P.K. Chattaraj, D.R. Roy, Update 1 of: electrophilicity index, Chemical Reviews. 107 (2007) PR46-PR74.
[38] R. Parthasarathi, J. Padmanabhan, M. Elango, et al., Intermolecular reactivity through the generalized philicity concept, Chemical Physics Letters. 394 (2004) 225–230.
[39] R. Vijayaraj, V. Subramanian, P. Chattaraj, Comparison of global reactivity descriptors calculated using various density functionals: a QSAR perspective, Journal of Chemical Theory and Computation. 5 (2009) 2744–2753.

[40] J. Padmanabhan, R. Parthasarathi, V. Subramanian, et al., Electrophilicity-based charge transfer descriptor, The Journal of Physical Chemistry a. 111 (2007) 1358–1361.
[41] D. Chakraborty, P.K. Chattaraj, Conceptual density functional theory based electronic structure principles, Chemical Science. 12 (2021) 6264–6279.
[42] S.U. Rehman, Z. Ding, Enhanced electronic and optical properties of three TMD heterobilayers, Physical Chemistry Chemical Physics. 20 (2018) 16604–16614.
[43] S.U. Rehman, J. Wang, G. Wu, et al., Unraveling the photocatalytic potential of transition metal sulfide and selenide monolayers for overall water splitting and photo-corrosion inhibition, Journal of Materials Chemistry a. 12 (2024) 6693–6702.
[44] W. Rahmalia, J.-F. Fabre, T. Usman, et al., Aprotic solvents effect on the UV–visible absorption spectra of bixin, Spectrochimica Acta Part a: Molecular and Biomolecular Spectroscopy. 131 (2014) 455–460.
[45] A.J. Morris, R.J. Nicholls, C.J. Pickard, et al., OptaDOS: A tool for obtaining density of states, core-level and optical spectra from electronic structure codes, Computer Physics Communications. 185 (2014) 1477–1485.
[46] A. Sharif, S. Jabeen, S. Iqbal, et al., Tuning the optoelectronic properties of dibenzochrysene (DBC) based small molecules for organic solar cells, Materials Science in Semiconductor Processing. 127 (2021) 105689.
[47] S. Kraner, G. Prampolini, G. Cuniberti, Exciton binding energy in molecular triads, The Journal of Physical Chemistry c. 121 (2017) 17088–17095.
[48] Z. Zhang, Q. Wu, D. Deng, et al., The post-treatment effects on open circuit voltages and device performances in a high efficiency all-small-molecule organic solar cell, Journal of Materials Chemistry c. 8 (2020) 15385–15392.
[49] Y. Yan, Y. Zhang, Y. Liu, et al., Simultaneously decreasing the bandgap and Voc loss in efficient ternary organic solar cells, Advanced Energy Materials. 12 (2022) 2200129.
[50] Z. Zheng, H. Yao, L. Ye, et al., PBDB-T and its derivatives: A family of polymer donors enables over 17% efficiency in organic photovoltaics, Materials Today. 35 (2020) 115–130.
[51] M.C. Scharber, D. Mühlbacher, M. Koppe, et al., Design rules for donors in bulk-heterojunction solar cells—Towards 10% energy-conversion efficiency, Advanced Materials. 18 (2006) 789–794.
[52] Z. Liu, T. Lu, Q. Chen, An sp-hybridized all-carboatomic ring, cyclo[18]carbon: Electronic structure, electronic spectrum, and optical nonlinearity, Carbon. 165 (2020) 461–467.